Effect of Plate Length on Construct Stiffness and Strain in a Synthetic Short-Fragment Fracture Gap Model Stabilized with a 3.5-mm Locking Compression Plate

Fabian N. Trefny[1] Mark Glyde[1] Giselle Hosgood[1] Alex Hayes[2] Robert Day[2]

[1] Division of Health Sciences, School of Veterinary Medicine, Murdoch University, Perth, Western Australia, Australia
[2] Department of Medical Engineering and Physics, Royal Perth Hospital, Perth, Australia

Address for correspondence Fabian N. Trefny, BVSc, School of Veterinary Medicine, Murdoch University, Perth, Western Australia 2106, Australia (e-mail: fabianntrefny@gmail.com).

Vet Comp Orthop Traumatol 2025;38:63–70.

Abstract

Objective To evaluate the effect of 3.5-mm locking compression plate (LCP) length on construct stiffness and plate and bone model strain in a synthetic, short-fragment, fracture-gap model.

Study Design Six replicates of 6-hole, 8-hole, 10-hole, and 12-hole LCP constructs on a short-fragment, tubular Delrin fracture gap model underwent four-point compression and tension bending. Construct stiffness and surface strain, calculated using three-dimensional digital image correlation, were compared across plate length and region of interest (ROI) on the construct.

Results The 12-hole plates (80% plate–bone ratio) had significantly higher construct stiffness than 6-hole, 8-hole, and 10-hole plates and significantly lower plate strain than 6-hole plates at all ROIs. Strain on the bone model was significantly lower in constructs with 10-hole and 12-hole plates than 6-hole plates under both compression and tension bending.

Conclusion Incremental increases in construct stiffness and incremental decreases in plate strain were only identified when comparing 6-hole, 8-hole, and 10-hole plates to 12-hole plates, and 6-hole to 12-hole plates, respectively. Strain on the bone model showed an incremental decrease when comparing 6-hole to 10-hole and 12-hole plates. A long plate offered biomechanical advantages of increased construct stiffness and reduced plate and bone model strain, over a short plate in this in vitro model.

Keywords
- plate length
- strain
- working length
- locking compression plate

Introduction

Planning fracture repair with plate fixation requires decision making on plate size, screw number, screw position, working length, and plate standoff distance, all affecting construct stiffness.[1–3] Validated guidelines for determining an ideal plate length have not been published but one proposal is based on the plate-span ratio and the plate-screw density.[4] The plate-span ratio is the quotient of the plate length and fracture length. The plate-screw density is the quotient of the number of plate screws and the number of available plate holes. In addition, a plate–bone ratio may be used to describe plate length, which is defined as the quotient of plate length and bone length.

Use of a long plate has been suggested to offer biomechanical advantages of high construct stiffness and strength, and

received
February 27, 2024
accepted after revision
August 6, 2024
article published online
August 21, 2024

Georg Thieme Verlag KG,
Rüdigerstraße 14,
70469 Stuttgart, Germany

DOI https://doi.org/10.1055/s-0044-1789263.
ISSN 0932-0814.

low plate strain.[1,2,5–7] In a plated bone, the plate length will determine the proportion of bone shielded by the plate, and differences in stiffness between plate-shielded and non-shielded bone will influence the distribution of strain.[8] Bone remodeling and in some cases peri-implant fracture are recognized clinically as manifestations of bone stress concentration at the plate end.[9–12] Despite this, studies on the effect of plate length on bone strain are lacking.

The aim of this study was to compare construct stiffness, plate strain, and strain in the bone model adjacent to the plate end of four different plate lengths using a synthetic, short-fragment, fracture gap model stabilized with a 3.5-mm locking compression plate (LCP). We hypothesized under both compression and tension bending, there would be incremental increases in construct stiffness with increases in plate length, and incremental decreases in plate and bone model strain with increases in plate length.

Materials and Methods

Bone Models

A synthetic, short-fragment, fracture-gap model was used. The bone model was constructed using acetal polymer tubes (Delrin: Mulford Plastics, Balcatta, WA, Australia) with an outer diameter of 15.9 mm and am inner diameter of 9.5 mm as used in previous biomechanical studies.[13,14] Six screw-holes and one jig-positioning hole on each end of the Delrin were predrilled on axial midline using a numerically controlled mill with a 2.8-mm drill bit (2.8-mm Drill Bit, Quick Coupling, 165 mm; Synthes GmbH, Oberdorf, Switzerland) as per AO recommendations (AO Foundation, Davos, Switzerland) for placement of 3.5-mm locking screws. Delrin was sectioned into 197-mm lengths and cut at an angle of 30 degrees to the long axis, generating a short segment of 45 mm, a long segment of 150 mm, and a fracture gap of 1.75 mm, modelling an imperfectly reduced, noncompressible, short-fragment diaphyseal fracture.

Construct Assembly

Six replicates of constructs with four plate lengths (24 constructs in total) were assembled, with a 6-hole, 8-hole, 10-hole, and 12-hole, 3.5-mm LCP (LCP: Synthes GmbH, Oberdorf, Switzerland) applied to the bone models (►**Fig. 1**). All constructs were assembled in random order by one board-certified surgeon (M.G.) using standard AO technique (AO Foundation, Davos, Switzerland) and maintaining a 1-mm plate standoff distance with a spacer (Tiling spacers, 1 mm, Rubi, Spain). Six 26-mm bicortical locking

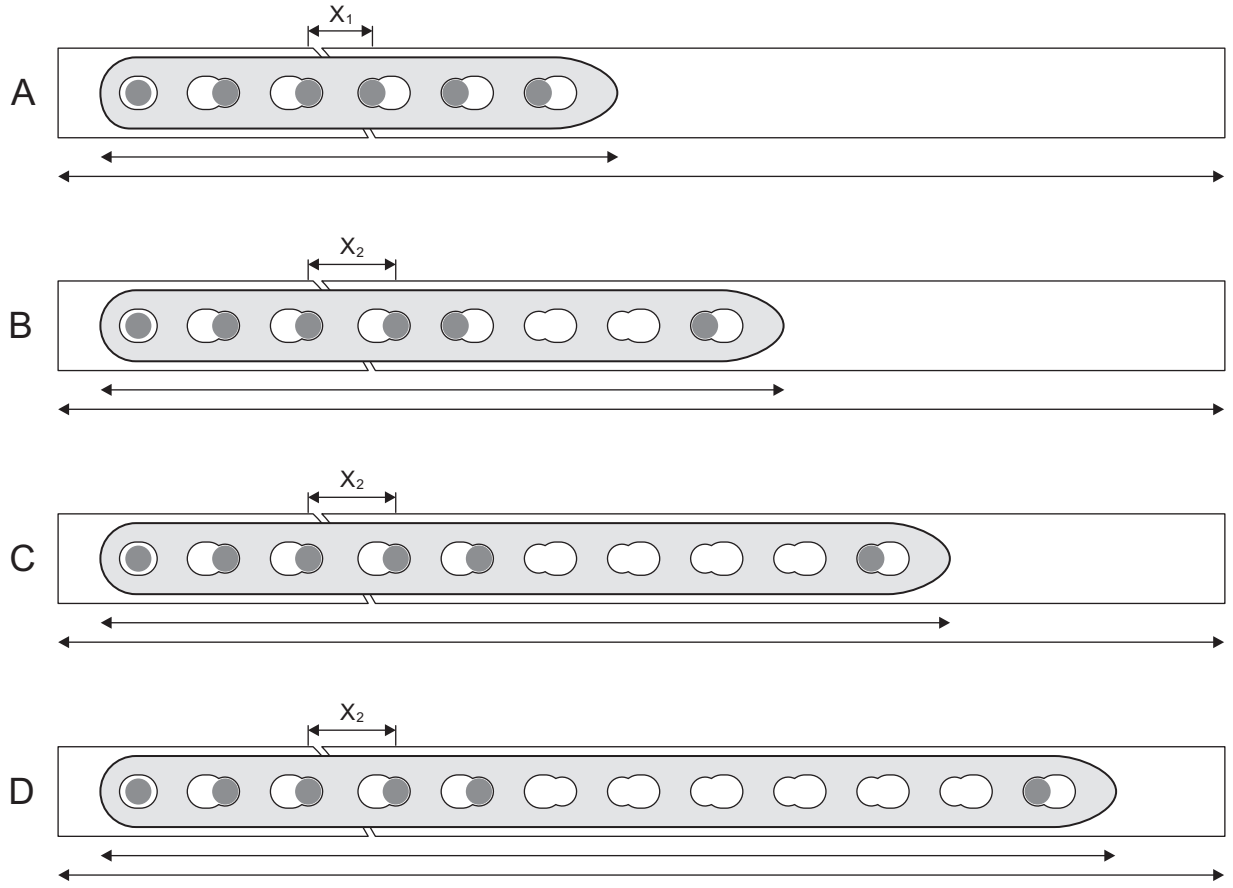

Fig. 1 Illustration depicting (**A**) 6-hole, (**B**) 8-hole, (**C**) 10-hole, and (**D**) 12-hole locking compression plate (LCP) constructs. The short oblique fracture gap is positioned between the third and fourth plate holes (left to right). Working length was lower in the 6-hole constructs (X_1) than the remaining constructs (X_2) due to differing plate hole layout over the fracture gap, such that $X_1 < X_2$. Arrows below each construct depict plate length relative to bone model length to calculate plate–bone ratio. Plate–bone ratios of the 6-hole, 8-hole, 10-hole, and 12-hole LCP constructs were 40, 53, 65, and 80%, respectively. Solid circles depict locked screw positions in the plate.

screws (Veterinary Locking Stardrive, 3.5-mm, Self-Tapping; Synthes GmbH, Oberdorf, Switzerland) were placed per construct using an orthopaedic drill (Cordless Driver III: Stryker Instruments, Kalamazoo, Michigan, United States) coupled with a 1.5-Nm torque limiter (Torque Limiter, 1.5 Nm, with AO/ASIF Quick Coupling: Synthes GmbH, Oberdorf, Switzerland) and screwdriver (Star Drive Screwdriver Shaft T15 with AO/ASIF Quick Coupling: Synthes GmbH, Oberdorf, Switzerland). In all constructs, three screws were placed in the short fragment, two screws were placed immediately adjacent to the fracture gap in the long fragment, and the sixth screw was placed at the end of the plate in the long fragment.

Working Length and Plate–Bone Ratio

Working length was defined as the distance between the innermost plate screws either side of the fracture gap,[15] under a 1-mm plate standoff distance. The working length differed between 6-hole plates and the remaining plate lengths due to differences in the combination-hole layout at the plate center (►**Fig. 1**). The working length was 9.4 mm for the 6-hole plates and 13 mm for all others. The plate–bone ratio of the 6-hole, 8-hole, 10-hole, and 12-hole LCP constructs was 40, 53, 65, and 80%, respectively (►**Fig. 1**).

Biomechanical Testing

Constructs were seated in a custom loading jig with a 3.5-mm bolt placed in each jig-positioning hole. Four-point bending was applied in two different planes sequentially, using a material testing machine (Instron 5566: Instron, Canton, Massachusetts, United States). Constructs were preloaded between support and load rollers with a 336- and 230-mm spacing, respectively, and subjected to nondestructive, quasi-static ramp loading for three cycles as per previously published protocol.[13,14,16–19] Three loading cycles were chosen based on pilot testing, which found no differences after the initial loading cycle. Load was applied using a 2 kN load cell in a direction parallel to the screw axis under displacement control (10 mm/minute) to a maximum force of 240 N (load range 0–240 N), producing a peak bending moment of 6 Nm. The position of load and support rollers was sequentially altered to enable both compression (gap opening) and tension (gap-closing) bending (►**Fig. 2**).

Measurement of Stiffness

Construct stiffness (N/mm) was derived from the slope of the linear (elastic) portion of the load displacement curve using Bluehill (Bluehill v2.5.391: Instron, Canton, Massachusetts, United States) between 150 and 240 N with a 10 Hz sampling frequency.

Measurement of Strain

Assembled constructs were painted with white (Flat White: White Knight, New South Wales, Australia) followed by a fine black speckle spray pattern (Flat Black: White Knight, New South Wales, Australia) to enable optical measurement of

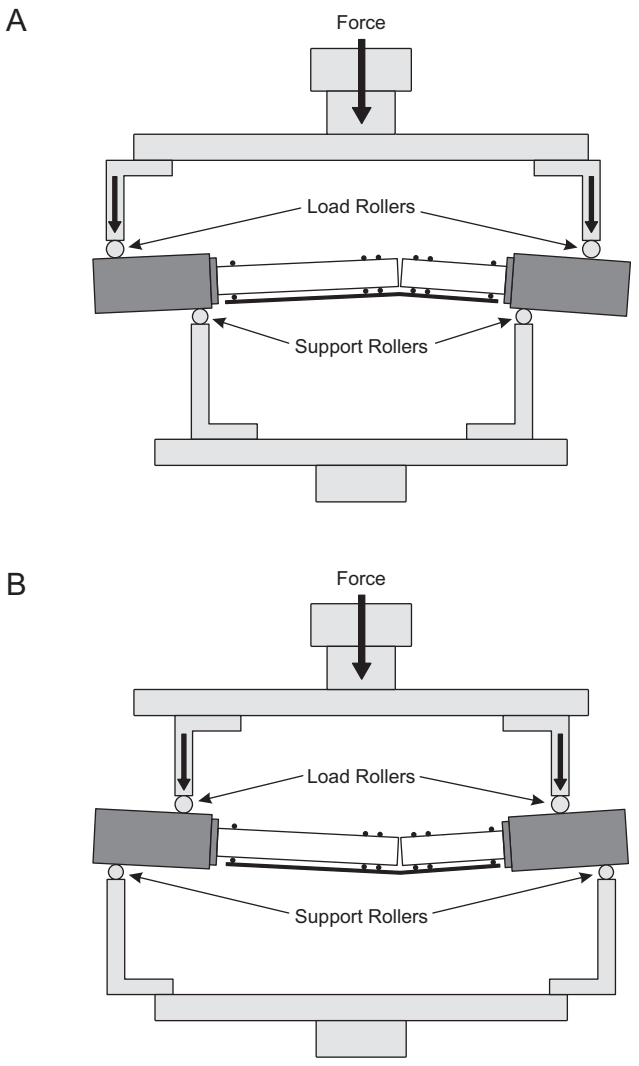

Fig. 2 Illustration of an assembled construct positioned in loading jigs positioned between load (upper) and support (lower) rollers. The position of load and support rollers is sequentially altered to enable both (**A**) compression (gap opening) and (**B**) tension (gap closing) four-point bending. Under both bending modes, plates remained positioned on the undersurface of the bone model, enabling optical measurement of von Mises strain below the construct.

von Mises strain using three-dimensional digital image correlation as previously described.[14,16–24] von Mises strain was calculated at six pre-defined regions of interest (ROIs) on the plate surface and one ROI on the bone model adjacent to the plate end (►**Fig. 3**). Stereo image displacements were obtained using two calibrated high-resolution cameras (Point Gray; Sony ICX625, Richmond, Canada) with $2{,}448 \times 2{,}048$ pixel sensors, converging at 60 degrees and operated at an exposure of 11 milliseconds. Correlation-based displacements of image subsets of the speckle pattern were captured using VicSnap (VicSnap, Correlated Solutions, South Carolina, United States). Post-hoc evaluation of displacements and calculation of von Mises strain was performed using VIC3D (VIC3D, Correlated Solutions, South Carolina, United States). Load (N) was plotted against von Mises strain and a line of best fit was used to calculate peak strain at a load of 240 N.

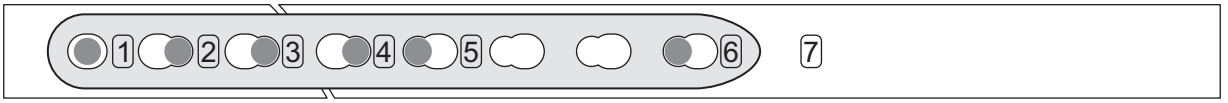

Fig. 3 Illustration depicting regions of interest (ROI) on an 8-hole locking compression plate (LCP) construct. The short oblique fracture gap is positioned between the third and fourth plate holes (left to right). Numbered boxes depict ROI for strain measurement (ROI 1–6 are positioned axially on the LCP surface; ROI 7 is positioned on the bone model adjacent to the plate end). Solid circles depict locked screw positions in the plate.

Statistical Methods

Statistical analysis was performed using SAS v9.8 (SAS Institute, North Carolina, United States). A sample size of six replicates across four plate lengths was sufficient to detect an effect size as small as 1.75, at a power of 0.8 and α at 0.05. The responses of interest were construct stiffness (N/mm) and strain (mm/mm) at each ROI in four-point bending. Responses were found to follow a normal distribution using the Shapiro–Wilk test, with failure to reject the null hypothesis of normality at $p \leq 0.05$. Responses were summarized as mean and 95% confidence interval. One-factor analysis of variance tested the effect of plate length on construct stiffness and two-factor analysis of variance tested the effect of plate length and ROI on plate and bone model strain. A two-sided research hypothesis was tested against the null hypothesis of no difference. Where there was a significant effect of plate length (one way) and interaction (two-way), planned pairwise comparisons were made between plate lengths or across ROIs against a Tukey-adjusted $p \leq 0.05$.

Results

Construct Stiffness

Under compression bending, construct stiffness was significantly higher for 12-hole plates than 6-hole ($p < 0.0001$), 8-hole ($p = 0.0037$), and 10-hole ($p = 0.0022$) plates, with no significant incremental increases in stiffness between 6-hole and 8-hole plates, 6-hole and 10-hole plates, or 8-hole and 10-hole plates (►**Table 1**). Under tension bending, construct stiffness was significantly higher for 12-hole plates than 6-hole ($p < 0.0001$), 8-hole ($p = 0.0015$), and 10-hole ($p = 0.0088$) plates with no significant incremental increases in construct stiffness between 6-hole and 8-hole plates, 6-hole and 10-hole plates, or 8-hole and 10-hole plates (►**Table 1**).

Plate Strain

Under compression bending, strain was significantly lower for 12-hole plates than 6-hole plates at all ROI ($p < 0.05$; ►**Table 2**). Strain was also significantly lower for 12-hole plates than 8-hole plates at ROI 1 ($p = 0.0138$) and 5 ($p = 0.0009$), and 10-hole plates at ROI 1 ($p = 0.0024$), 3 ($p = 0.0228$), and 5 ($p = 0.0373$). Under tension bending, strain was significantly lower for 12-hole plates than 6-hole plates at all ROI ($p < 0.05$; ►**Table 3**). Strain was also significantly lower for 12-hole plates than 8-hole plates at ROI 2 ($p = 0.0005$), and 10-hole plates at ROI 1 ($p = 0.0267$), 2 ($p = 0.0001$), 3 ($p = 0.0333$), and 6 ($p = 0.0035$). Under both compression and tension bending, the 12-hole plates did not have significantly higher strain than other plates at any ROI.

Strain in the Bone Model

Under compression bending, strain was significantly lower for 12-hole ($p = 0.0073$) and 10-hole ($p = 0.0196$) plates than 6-hole plates at the ROI on the bone model adjacent to the plate end (ROI 7; ►**Table 2**). There was no significant difference between 12-hole and 10-hole plates at ROI 7 ($p = 0.8489$). Under tension bending, strain was significantly lower for 12-hole plates than 6-hole ($p < 0.0001$), 8-hole ($p < 0.0001$), and 10-hole ($p = 0.0066$) plates at ROI 7 (►**Table 3**). Strain was also significantly lower for 10-hole plates than 6-hole ($p < 0.0001$) and 8-hole ($p < 0.0040$) plates, and for 8-hole plates than 6-hole ($p = 0.0001$) plates.

Discussion

This study investigated, using an in vitro bone model, the effect of plate length on construct stiffness, plate strain, and strain at the ROI on the bone model adjacent to the plate end. Our first research hypothesis of incremental increases in construct stiffness with increases in plate length was only accepted when comparing 6-hole, 8-hole, or 10-hole to 12-

Table 1 Mean (95% confidence interval) construct stiffness (N/mm) under compression and tension bending

Construct	Compression bending, N/mm	Tension bending, N/mm
6-hole	61.7[a] (56.9–66.5)	58.5[a] (54.7–62.4)
8-hole	66.1[a] (61.9–70.4)	62.3[a] (57.7–66.9)
10-hole	65.6[a] (63.9–67.4)	64.3[a] (59.7–68.8)
12-hole	74.5[b] (70.7–78.4)	73.4[b] (68.2–78.6)

Note: Within a column, means with the same superscript ([a, b]) are not significantly different (Tukey-adjusted $p > 0.05$).

Table 2 Mean (95% confidence interval) strain (mm/mm) at each numbered region of interest (ROI) under four-point compression bending

LCP construct	ROI 1	2	3	4	5	6	7
6-hole	95.94[a] (88.52–103.36)	90.65[a] (49.35–131.95)	50.80[a] (42.33–59.26)	23.39[a] (16.46–30.32)	12.72[a] (10.99–14.45)	116.33[a] (102.61–130.04)	271.84[a] (239.98–303.69)
8-hole	76.29[a] (67.03–85.55)	69.58[a,b] (54.96–84.21)	49.20[a,b] (44.20–54.21)	21.16[a,b] (19.69–22.63)	12.27[a] (10.27–14.27)	135.30[a,b] (82.37–188.23)	239.64[a,b] (222.14–257.14)
10-hole	79.35[a] (68.62–90.07)	69.80[a,b] (60.39–79.22)	51.15[a] (42.65–59.65)	19.08[a,b] (17.37–20.79)	10.78[a] (9.13–12.43)	92.54[a,b] (74.30–110.79)	216.05[b] (172.25–259.86)
12-hole	59.77[b] (56.00–63.54)	38.53[b] (33.34–43.72)	39.43[b] (36.08–42.78)	15.72[b] (11.98–19.46)	8.18[b] (7.39–8.97)	67.89[b] (41.81–82.05)	200.67[b] (173.47–227.86)

Note: Within each column, means with the same superscript ([a, b]) are not significantly different (Tukey-adjusted $p > 0.05$).

Table 3 Mean (95% confidence interval) strain (mm/mm) at each numbered region of interest (ROI) under four-point tension bending

LCP construct	ROI 1	2	3	4	5	6	7
6-hole	92.07[a] (77.11–107.02)	82.67[a] (76.25–89.10)	60.77[a] (56.18–65.35)	24.77[a] (17.62–31.92)	13.97[a] (9.22–18.73)	130.30[a] (99.28–161.33)	318.53[a] (300.89–336.18)
8-hole	75.13[a,b] (67.49–82.76)	63.42[a] (58.59–68.24)	54.98[a,b] (43.06–66.89)	20.95[a,b] (12.21–29.69)	13.23[a,b] (9.97–16.49)	102.14[a,b] (68.44–135.84)	265.39[b] (257.28–273.51)
10-hole	78.62[a] (70.36–86.89)	65.75[a] (57.22–74.27)	62.51[a] (54.37–70.64)	20.30[a,b] (16.77–23.83)	12.98[a,b] (9.58–16.37)	138.60[a] (124.82–152.39)	227.12[c] (201.99–252.25)
12-hole	61.39[b] (53.73–69.05)	42.99[b] (33.14–52.83)	49.66[b] (42.27–57.05)	14.80[b] (11.46–18.14)	8.78[b] (7.33–10.23)	74.26[b] (41.75–106.76)	190.98[d] (175.78–206.18)

Note: Within each column, means with the same superscript ([a, b, c, d]) are not significantly different (Tukey-adjusted $p > 0.05$).

hole plates, corresponding to 40, 53, and 65% to 80% plate–bone ratio, respectively.

A previous biomechanical investigation also reported significantly higher stiffness in 12-hole plates compared with 8-hole plates under axial compression and torsion in a synthetic, small-gap finite element model stabilized with a 4.5-mm titanium LCP.[2] In our study, bending remained within the linear region of the load displacement curve. Other studies reported higher yield strength of 10-hole versus 8-hole LCP constructs during four-point bending,[25] whereas studies employing dynamic compression plate constructs reported higher bending strength when using longer plates with fewer screws.[7,26] In these studies, constructs were tested beyond the yield point, defined as the change from elastic to plastic deformation,[15,27] illustrating that biomechanical advantages of using a long plate remained beyond material elastic limits.

Our research hypothesis of an incremental decrease in plate strain with an increase in plate length was only accepted when comparing 6-hole to 12-hole plates. This effect was seen at all ROIs, including the ROI immediately over the fracture gap. At no ROI was strain significantly higher for a longer plate than a shorter plate. We did not perform fatigue testing, so it is not possible to make claims about plate length and fatigue failure. However, when loading occurs within elastic limits, such as in fatigue, implant stress is proportional to implant strain, and small increases in implant stress are known to significantly shorten implant fatigue life.[28,29] For this reason, any decisions on plate selection, such as plate length, that reduce implant strain may thereby also reduce the risk of fatigue failure.

Our research hypothesis of an incremental decrease in strain at the ROI on the bone model adjacent to the plate end with an increase in plate length was only accepted when comparing the 6-hole to the 10-hole and 12-hole plates. Lower strain observed in the bone model at the plate end may be explained by the relative decrease in the external force lever arm as the plate–bone ratio increases with an expected, consequent reduction in the stress concentration in the bone model.[11,12] These findings illustrate potential clinical implications of selecting plate length on stress concentration in the nonplated bone region as has been previously described.[9,10,12]

In this study, incremental increases in construct stiffness and decreases in plate strain were only identified when comparing plate–bone ratios of 40, 53, and 65% to 80% and between 40 and 80%, respectively. Failure to detect significant differences with smaller changes in plate–bone ratio may suggest that a threshold plate–bone ratio is necessary before significant biomechanical differences are apparent. The sequential increase in plate–bone ratio from the 10-hole to 12-hole plates represented an increment of 15%, compared with a sequential increment of 12 and 13% from the 8-hole to 10-hole and 6-hole to 8-hole plates, respectively. Alternatively, these results may reflect type II error, with power insufficient to detect the smaller difference in light of the variance between replicates. Performing multiple comparisons can magnify this error, for example, comparing across ROIs, testing against conservative criteria for type I error. Our sample size of six replicates per treatment group was sufficient to detect an effect size as small as 1.75, based on previous investigations using a similar experimental design.[13,14] One advantage of the synthetic model is its uniformity and the low variability that is generated between replicates, extending confidence around reducing type II error. However, given that the mean effect size that remained undetected in this study ranged from 0.5 to 1, requiring a sample size of 17 to 50, it is possible some results could reflect type II error.

Guidelines for fracture repair were met in construction of this model, including a minimum of three locked screws per fragment using a screw configuration based on AO recommendations.[1,2,6,30] An inherent difficulty with the model was the inability to maintain a consistent working length across all constructs, despite maintaining a constant screw configuration. The 3.5-mm LCP features 13-mm spacing between the locking part of the combination holes, except for the spacing between locking holes at either side of the plate center, where locking holes are spaced 9.4 mm apart.[31] The eccentric location of the fracture gap in our model, and LCP combination-hole layout at the plate center, resulted in a 9.4-mm working length for the 6-hole plates and a 13-mm working length for the remaining plates, representing a 38% increase in working length. Previous investigations have reported that increasing working length decreases construct stiffness and increases plate strain.[2,13,14,16–19,32] Therefore, working length may have confounded or mitigated the change expected for the 8-hole and 10-hole plates, which may not have been overcome until the plate–bone ratio reached 80% for the 12-hole plates.

Use of short plates has been recommended to minimize soft tissue dissection and obviate disruption to fracture biology.[33,34] However, in vitro, shorter plates have been shown to have lower axial stiffness[2] and bending strength.[7,26] The biologic consequences of using long plates can be overcome, in part, by the minimally invasive application of longer plates with lower plate screw densities. Minimally invasive plate application preserves fracture biology while minimizing morbidity associated with traditional open approaches.[15,35–37] Choosing a longer plate may therefore be less restricted by fracture biology and better, based on the plate–bone ratio, to achieve maximum biomechanical advantage.

The plate-span ratio and plate-screw density as previously described[4] may be less useful criteria for deciding on ideal plate length in simple fractures with small fracture gaps due to ambiguity surrounding measurement of fracture length, and in patients with short limb segments that mandate use of short plates. Guidelines derived from results in humans suggest a minimum plate-span ratio greater than 8 to 10 and a plate-screw density of less than 0.3 to 0.4 are necessary for simple fractures such as the configuration modeled in our study.[1,4] These suggestions were, however, derived retrospectively from outcomes of fracture repair in people. When considering the 1.75-mm fracture gap modeled in our study, the calculated plate-span ratio in the 6-hole 3.5-mm LCP

(measuring 79 mm in length) would equate to 45, which is far in excess of the minimum recommended guideline. Despite meeting this criterion, the 6-hole plates were significantly less stiff and had significantly higher plate strain than the 12-hole plates. Furthermore, achieving a plate-screw density of less than one is not clinically feasible when using a 6-hole plate while also satisfying the recommendation of three screws per fragment. While it was shown that construct stiffness is proportional to plate length and therefore plate–bone ratio, the ideal construct stiffness remains unknown, and was beyond the scope of our study.

A simple short-fragment, oblique, small fracture gap was modeled in this study as this fracture configuration occurs commonly in veterinary patients and is challenging to repair in vivo since the oblique fracture configuration usually prevents axial compression with a bone plate. Axial compression of transverse and suitably short oblique fractures with compression plating has the intent and potential to eliminate fracture gap and increase construct stiffness through frictional contact of the fracture ends, thereby also decreasing plate strain.[30,33] Four-point bending was used to generate a uniform bending moment across all constructs.[38] While axial and torsional loading of constructs was not performed, in this instance, bending represents the most biomechanically relevant load acting on long bones with eccentrically positioned plates.[39,40]

In our model, under both compression and tension bending, incremental increases in construct stiffness and decreases in plate strain were identified between the 6-hole, 8-hole, and 10-hole plates to 12-hole plates, and between 6-hole and 12-hole plates, respectively. Under both compression and tension bending, strain at the ROI on the bone model adjacent to the plate end only showed incremental decreases from 6-hole to 10-hole and 12-hole plates. Our results showed that a long plate offers the biomechanical advantages of high construct stiffness and low plate and bone model strain. While a long plate was shown to biomechanically outperform a short plate in this context, consideration must also be given to other factors when guiding selection of plate length in clinical cases, including fracture location, configuration, and potential consequences on fracture biology.

Note

An abstract of this paper was presented at the annual European College of Veterinary Surgeons Congress, July 6, 2019, Budapest, Hungary. Results from this study were also presented at the AO Vet Symposium, Bridging the Gap: Translating Clinical Research to Clinical Practice, presented November 23, 2020, via Webinar.

Authors' Contribution

All authors contributed to the conception and design of this study. F.T., M.G., R.D., and A.H. were involved with data acquisition and material testing. R.D. and A.H. provided technical support with material testing and use of software. G.H. contributed to acquisition of data and data analysis. All authors contributed to data interpretation and revision of the submitted manuscript.

Funding

The authors received partial financial support for the implants from DePuy Synthes.

Conflict of Interest

None declared.

Acknowledgement

The authors wish to thank DePuy Synthes for partial financial support through provision of implants and to the Royal Perth Hospital for access to engineering and material testing laboratory.

References

1 Gautier E, Sommer C. Guidelines for the clinical application of the LCP. Injury 2003;34(Suppl 2):B63–B76
2 Stoffel K, Dieter U, Stachowiak G, Gächter A, Kuster MS. Biomechanical testing of the LCP–how can stability in locked internal fixators be controlled? Injury 2003;34(Suppl 2):B11–B19
3 Wagner M. General principles for the clinical use of the LCP. Injury 2003;34(Suppl 2):B31–B42
4 Rozbruch SR, Müller U, Gautier E, Ganz R. The evolution of femoral shaft plating technique. Clin Orthop Relat Res 1998;(354): 195–208
5 Beltran MJ, Collinge CA, Gardner MJ. Stress modulation of fracture fixation implants. J Am Acad Orthop Surg 2016;24(10): 711–719
6 Miller DL, Goswami T. A review of locking compression plate biomechanics and their advantages as internal fixators in fracture healing. Clin Biomech (Bristol, Avon) 2007;22(10): 1049–1062
7 Sanders R, Haidukewych GJ, Milne T, Dennis J, Latta LL. Minimal versus maximal plate fixation techniques of the ulna: the biomechanical effect of number of screws and plate length. J Orthop Trauma 2002;16(03):166–171
8 Gautier E, Perren SM, Cordey J. Strain distribution in plated and unplated sheep tibia an in vivo experiment. Injury 2000;31 (Suppl 3):C37–C44
9 Akeson WH, Woo SLY, Rutherford L, Coutts RD, Gonsalves M, Amiel D. The effects of rigidity of internal fixation plates on long bone remodeling. A biomechanical and quantitative histological study. Acta Orthop Scand 1976;47(03):241–249
10 Chan LWM, Gardner AW, Wong MK, Chua K, Kwek EBKSingapore Orthopaedic Research CollaborativE (SORCE) Non-prosthetic peri-implant fractures: classification, management and outcomes. Arch Orthop Trauma Surg 2018;138(06):791–802
11 Davenport SR, Lindsey RW, Leggon R, Miclau T, Panjabi M. Dynamic compression plate fixation: a biomechanical comparison of unicortical vs bicortical distal screw fixation. J Orthop Trauma 1988;2(02):146–150
12 Park KC, Lim SJ, Song YS, Hwang KT. Factors affecting periimplant fracture following locking plate for osteoporotic distal femur fractures. Orthop Traumatol Surg Res 2017;103(08): 1201–1204
13 Pearson T, Glyde M, Hosgood G, Day R. The effect of intramedullary pin size and monocortical screw configuration on locking compression plate-rod constructs in an in vitro fracture gap model. Vet Comp Orthop Traumatol 2015;28(02):95–103
14 Pearson T, Glyde MR, Day RE, Hosgood GL. The effect of intramedullary pin size and plate working length on plate strain in locking compression plate-rod constructs under axial load. Vet Comp Orthop Traumatol 2016;29(06):451–458
15 Chao P, Lewis DD, Kowaleski MP, Pozzi A. Biomechanical concepts applicable to minimally invasive fracture repair in small animals. Vet Clin North Am Small Anim Pract 2012;42(05):853–872, v

16 Bird G, Glyde M, Hosgood G, Hayes A, Day R. Effect of plate type and working length on a synthetic compressed juxta-articular fracture model. VCOT Open 2020;03(02):e119–e128
17 Bird G, Glyde M, Hosgood G, Hayes A, Day R. Biomechanical comparison of a notched head locking T-plate and a straight locking compression plate in a juxta-articular fracture model. Vet Comp Orthop Traumatol 2021;34(03):161–170
18 de Bruyn BW, Glyde M, Day R, Hosgood G. Effect of an orthogonal locking plate and primary plate working length on construct stiffness and plate strain in an in vitro fracture-gap model. Vet Comp Orthop Traumatol 2024;37(04):173–180
19 Evans A, Glyde M, Day R, Hosgood G. Effect of plate-bone distance and working length on 2.0-mm locking construct stiffness and plate strain in a diaphyseal fracture gap model: a biomechanical study. Vet Comp Orthop Traumatol 2024;37(01):1–7
20 Amin Yavari S, van der Stok J, Weinans H, Zadpoor AA. Full-field strain measurement and fracture analysis of rat femora in compression test. J Biomech 2013;46(07):1282–1292
21 Palanca M, Tozzi G, Cristofolini L. The use of digital image correlation in the biomechanical area: a review. Int Biomech 2016;3(01):1–21
22 Sztefek P, Vanleene M, Olsson R, Collinson R, Pitsillides AA, Shefelbine S. Using digital image correlation to determine bone surface strains during loading and after adaptation of the mouse tibia. J Biomech 2010;43(04):599–605
23 Väänänen SP, Amin Yavari S, Weinans H, Zadpoor AA, Jurvelin JS, Isaksson H. Repeatability of digital image correlation for measurement of surface strains in composite long bones. J Biomech 2013;46(11):1928–1932
24 Withers PJ. Strain measurement by digital image correlation. Strain 2008;44(06):421–422
25 Weiss DB, Kaar SG, Frankenburg EP, Karunakar MA. Locked versus unlocked plating with respect to plate length in an ulna fracture model. Bull NYU Hosp Jt Dis 2008;66(01):5–8
26 Törnkvist H, Hearn TC, Schatzker J. The strength of plate fixation in relation to the number and spacing of bone screws. J Orthop Trauma 1996;10(03):204–208
27 Golish SR, Mihalko WM. Principles of biomechanics and biomaterials in orthopaedic surgery. J Bone Joint Surg Am 2011;93(02): 207–212
28 Liu X, Zhang S, Bao Y, Zhang Z, Yue Z. Strain-controlled fatigue behavior and microevolution of 316L stainless steel under cyclic shear path. Materials (Basel) 2022;15(15):5362–5374
29 Sistaninia M, Niffenegger M. Fatigue crack initiation and crystallographic growth in 316L stainless steel. Int J Fatigue 2015; 70:163–170
30 Johnson AL, Houlton JEF, Vannini R. AO Principles of Fracture Management in the Dog and Cat. 1st ed. Vol 148;. Davos Platz, Switzerland: AO Publishing; 2005
31 Veterinary Product Catalog Implants. Instruments, Sets. DePuy Synth Vet; 2017. Accessed August 13, 2021 at: https://catalog.synthes.com/getprg.ch?catalogId=VET&chapterId=VET_02&systemId=S_VET_0202.004&programId=S_VET_0200.004.03
32 MacLeod AR, Serrancoli G, Fregly BJ, Toms AD, Gill HS. The effect of plate design, bridging span, and fracture healing on the performance of high tibial osteotomy plates: an experimental and finite element study. Bone Joint Res 2019;7(12): 639–649
33 Niemeyer P, Südkamp NP. Principles and clinical application of the locking compression plate (LCP). Acta Chir Orthop Traumatol Cech 2006;73(04):221–228
34 Perren SM. Evolution of the internal fixation of long bone fractures. The scientific basis of biological internal fixation: choosing a new balance between stability and biology. J Bone Joint Surg Br 2002;84(08):1093–1110
35 Garofolo S, Pozzi A. Effect of plating technique on periosteal vasculature of the radius in dogs: a cadaveric study. Vet Surg 2013;42(03):255–261
36 Pozzi A, Lewis D. Surgical approaches for minimally invasive plate osteosynthesis in dogs. Vet Comp Orthop Traumatol 2009;22(04): 316–320
37 Pozzi A, Hudson CC, Gauthier CM, Lewis DD. Retrospective comparison of minimally invasive plate osteosynthesis and open reduction and internal fixation of radius-ulna fractures in dogs. Vet Surg 2013;42(01):19–27
38 Sharir A, Barak MM, Shahar R. Whole bone mechanics and mechanical testing. Vet J 2008;177(01):8–17
39 Maxwell M, Horstman CL, Crawford RL, Vaughn T, Elder S, McLaughlin R. The effects of screw placement on plate strain in 3.5 mm dynamic compression plates and limited-contact dynamic compression plates. Vet Comp Orthop Traumatol 2009;22(02): 125–131
40 Zahn K, Frei R, Wunderle D, et al. Mechanical properties of 18 different AO bone plates and the clamp-rod internal fixation system tested on a gap model construct. Vet Comp Orthop Traumatol 2008;21(03):185–194